

## HIERARCHICALLY POROUS $\text{Fe}_2\text{O}_3$ AND $\text{Fe}_2\text{O}_3/\text{SiO}_2$ COMPOSITES PREPARED BY CYPRESS TISSUE TEMPLATE WITH ASSISTANCE OF SUPERCRITICAL $\text{CO}_2$

Wei Ni, Qun Xu,\* Jian-Xia Jiao, Xiaofang Liu, and Chenxing Ren

Hierarchically porous  $\alpha\text{-Fe}_2\text{O}_3$  and silica-based  $\text{Fe}_2\text{O}_3$  composites (I & II) ranging from nanopores to micrometer-sized pores have been prepared by a nanoscale casting process, using cypress wood tissue template in supercritical carbon dioxide ( $\text{scCO}_2$ ). These wood-templated  $\text{Fe}_2\text{O}_3$  and its  $\text{SiO}_2$ -based composites with special hierarchical but continuous pore size from 9 nm up to 20  $\mu\text{m}$ , were prepared from  $\text{scCO}_2$  hybrid solution with cosolvent and precursor(s). Different characterization techniques such as SEM, XRD, and  $\text{N}_2$  adsorption-desorption were used to investigate the morphology and structure of  $\text{Fe}_2\text{O}_3$  and its composites in different length scales. The  $\text{Fe}_2\text{O}_3$  porous material showed a specific characteristic of being accumulated by  $\text{Fe}_2\text{O}_3$  granules in the size range ca. 100–200 nm. The  $\text{SiO}_2$ -based  $\text{Fe}_2\text{O}_3$  composites exhibited a BET area of 99–104  $\text{m}^2/\text{g}$ , which was much higher than that of pure  $\text{Fe}_2\text{O}_3$ ; this implies that the silica probably exists in the form of a gel skeleton.

*Keywords:* Supercritical carbon dioxide; Wood template; Iron oxide; Silica; Composite; Porous; Hierarchical

*Contact information:* College of Materials Science and Engineering, Zhengzhou University, Zhengzhou 450052, China. \*Corresponding author: Tel.: +86 371 67767827; Fax: +86 371 67763561; <mailto:qunxu@zzu.edu.cn>

### INTRODUCTION

Supercritical fluids (SCFs) have been the focus of much attention because of their unique properties of low viscosity, high diffusivity, and controllable solubility by changing the temperature and pressure or by adding a modifier (Cooper 2003; Johnston and Shah 2004; Darr and Poliakoff 1999). Among the SCFs, supercritical carbon dioxide ( $\text{scCO}_2$ ) is especially important because it is an easily handled green-solvent with nonflammable, nontoxic, inexpensive, and low critical temperature characteristics. Moreover,  $\text{scCO}_2$  is a nonpolar solvent that can dissolve most organic small molecules; thus, for example, it is expected to carry an ample quantity of precursors into the fine space of the substrate for many kinds of oriented or ordered materials. The novel process for material synthesis called “nanoscale casting using supercritical fluids (NC-SCF)” has been developed by Wakayama’s group for activated carbon-templated nanoporous materials (Fukushima and Wakayama 1999). The process also has been highlighted in the field of inorganic porous materials preparation (Cabañas et al. 2005).

As is well known, porous materials can have excellent physicochemical properties, including porous structures and specific surface characteristics, making them suitable for applications in adsorption, separation, catalysis, ion exchange, and chemical

sensing. Their fundamental properties can make such materials useful in a variety of areas including chemistry, physics, electronics, optics, material science, and biomedical science (Poliakoff et al. 2002; Cooper 2003; Ying et al. 1999). The hierarchically porous materials have potential applications in both highly selective absorbent products and facilitated mass transfer. The macroscopic shape of porous materials is also important for applications such as plastic molding or metal casting in industrial processes (Wakayama and Fukushima 2000). One typical method of building controlled or tailored structures is replication, including inverse, hollow, and true replication (Wakayama and Fukushima 1999). Materials from nature, such as wood tissue, can be morphologically complex, with sophisticated structure and ordering, and may provide an excellent natural template for a hierarchical porous structure (Tirrell et al. 1994). Wood-templated porous materials have been highlighted that are uniquely suited to the fabrication of meso- or macroporous materials with desirable macroscopic shapes (Dong et al. 2002; Wang et al. 2000).

Compared with traditional processes, the high mass-carrying power and controllable dissolvability of precursors in SCFs, but without harmful organic solvent residue, may give us a surprise in a preferable nanoscale casting. Based on our previous study on hierarchically porous silica by hardwood template (Ni et al. 2008), here we adopted the NC-SCF process and a softwood, cypress tissue, as template for the preparation of hierarchically porous Fe<sub>2</sub>O<sub>3</sub> and its composites with silica, which may have potential uses in catalysis (Chen and Sachtler 1998; Panov et al. 1998), lightweight or polymer-based composite magnets, electronics or battery fields, etc. (Cornell and Schwertmann 1996; Jolivet 2000).

## EXPERIMENTAL

### Materials

Materials included cypress slices (10×10×6 mm<sup>3</sup>), aqueous ammonia (AP, Luoyang Henghui Chem. Ltd.), HCl (AP, Kaifeng Kaihua reagent Ltd.), anhydrous FeCl<sub>3</sub> (CP, Guoyao group Chem. Ltd.), tetraethyl orthosilicate (TEOS, AP, Guoyao group Chem. Ltd.), dehydrated ethanol (AP, 99.7%, Anhui Ante biochemistry Ltd.), CO<sub>2</sub> (99.9%, Zhengzhou Shuangyang gas Co.), and deionized water.

### Main Apparatus and Instrument

A single cylinder injection pump (DB-80) was provided by Beijing Weixing Co. A stainless steel autoclave (50 ml), attached with electric heating collar and thermostatic controller, was supplied by Jiangsu Hai'an instrument plant. A muffle furnace (5-12) was from the Shenyang electric furnace plant.

### Experimental Process for Porous Materials

A porous iron oxide and silica-based iron oxide ceramics with a wood-like microstructure that was analogous to "silicified wood" were prepared. The production of "ironified wood" was performed using the following process: (i) introduction of iron chloride precursor or another co-precursor, i.e. TEOS, into wood tissue template or silicified wood template via scCO<sub>2</sub>/ethanol media, (ii) hydrolysis of the iron chloride

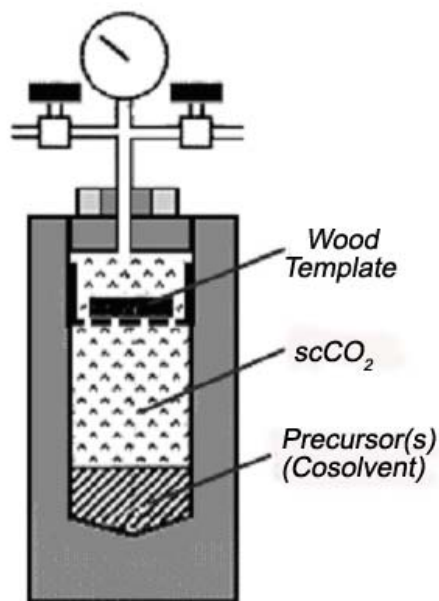
and/or TEOS precursor(s) in the cell structure to form an iron oxide or its composite gel, and (iii) calcining at a temperature of 600–1000°C in air. Then the resulting iron oxide or its composite ceramics would have inherited the external and internal forms of the original wood.

#### *Iron oxide porous material*

The typical process and conditions were as follows: The raw cypress wood was cut into slices and extracted by boiling aqueous ammonia twice, and then hydrochloric acid dilute solution, for purification before use. First, 5 mmol FeCl<sub>3</sub> was dissolved in 10 ml ethanol, and then placed in a stainless steel autoclave of 50-ml capacity. Then the prepared cypress tissue template was placed in a stainless steel cage fixed at the upper part of the autoclave without touching the FeCl<sub>3</sub>/ethanol solution at the bottom, as shown in Scheme 1. Later the cooled CO<sub>2</sub> was pumped into the autoclave, and the sample was treated at 10 MPa, 40 °C for 2 h. After depressurization, the sample was immersed in the ammoniac hydrolyzing solution (1.5 wt%) for 3 h, preceded by a few minutes of ultrasonic vibration. The hydrolyzed sample was dried at 80 °C for 8 h in ambient atmosphere. The cypress tissue template was then removed by calcination at 600 °C, 800 °C, or 1000 °C for 4 h in air.

#### *Iron oxide/silica porous composite (Fe/Si Method #1)*

The preparing process of iron oxide/silica porous composite was similar to that of iron oxide, but the FeCl<sub>3</sub>+EtOH solution in the autoclave was replaced by FeCl<sub>3</sub>+TEOS+EtOH solution (2.5mmol FeCl<sub>3</sub>+5ml TEOS+5ml ethanol), upgrading from the ternary system to a more complicated quaternary system.



**Scheme 1.** Schematic illustration of the autoclave and cage used to treat samples in scCO<sub>2</sub>.

### *Iron oxide coated porous silica*

The iron oxide coated porous silica was prepared by impregnating FeCl<sub>3</sub> (2.5 mmol FeCl<sub>3</sub>) both into silica-coated wood composite (Fe/Si Method #2) or porous silica thereof (Fe/Si Method #3). The other operations and conditions were analogous to the aforementioned.

### **Characterization for Porous Materials**

Nitrogen adsorption-desorption isotherms were obtained at 77 K and with an outgas temperature at 100 °C on a surface energy and pore size analyzing instrument of QUANTACHROME NOVA 1000e. The BJH (Barrett-Joyner-Halenda) method on the desorption branch was used to determine the mesopore size distribution. The crystalline phases for porous samples were identified with a RIGAKU MAX-III B diffractometer with Cu K $\alpha$  radiation in the range of 2 $\theta$ =10° to 80° in steps of 0.02°, at the rate of 6°(2 $\theta$ )/min. The SEM photographs were obtained using an FEI QUANTA 200 scanning electron microscope.

## **RESULTS AND DISCUSSION**

In this study the pressure of the supercritical system was mainly investigated, since in our previous work (Ni et al. 2008) the process was optimized with the following conclusions: 1) the scCO<sub>2</sub> showed a more powerful dissolvability with a lower temperature and higher pressure, 2) a high concentration of precursor and suitably long period were beneficial for the impregnation into the matrix. Several concepts used in the following analysis are identified as follows:

$$\text{coating ratio} = m_c / m_0 \quad (1)$$

$$\text{yield} = m_f / m_a \quad (2)$$

where  $m_0$  is the mass of dry cypress slice, and  $m_c$  is the coating mass of precursor and cosolvent ethanol into the cypress slice without further drying treatment,  $m_a$  represents the mass of dried cypress slice being impregnated, and  $m_f$  for the porous inorganic product after calcination. For a simplified and effective process, the system biphasic compatibility was first investigated under different pressures.

### **Compatibility of Fluid Phases**

During the scCO<sub>2</sub> assisted impregnation/coating process, the precursor should be soluble in CO<sub>2</sub>. Thus, when the solid solute is not soluble in SCF, as in this study, it is necessary to study the miscibility of CO<sub>2</sub> in the impregnation solution. In other words, information about the solubility of the solution phase in the SCF phase is needed. The high-pressure phase behavior of the hybrid solvent was measured, i.e. the cosolvent ethanol solubility in CO<sub>2</sub>. The extent of miscibility is reflected in the volume expansion of the liquid phase. The volume expansion of the liquid phase  $\Delta V$  at a certain pressure  $P$  and temperature  $T$  is defined by

$$\Delta V = [V(P, T_2) - V(P^0, T_1)] / [V_0 - V(P^0, T_1)] \quad (3)$$

where  $P^0$  represents the atmospheric pressure, and  $V_0$  for the capacity of windowed autoclave (50-ml in our experiment).

The compatibility of ethanol with CO<sub>2</sub> was investigated in a 50-ml stainless steel autoclave with quartz-windows. The result shows that the solvent power of CO<sub>2</sub> was enhanced with increasing pressure (illustrated in Fig. 1). It can be seen that the miscibility increased when the CO<sub>2</sub> pressure rose from 5 MPa up to 10 MPa, with the critically compatible pressure of ca. 8.5 MPa at 40 °C. As the EtOH cosolvent showed a very similar volumetric expansion behavior with its FeCl<sub>3</sub> solution in SCF phase, no further replications of this phenomenon are shown.

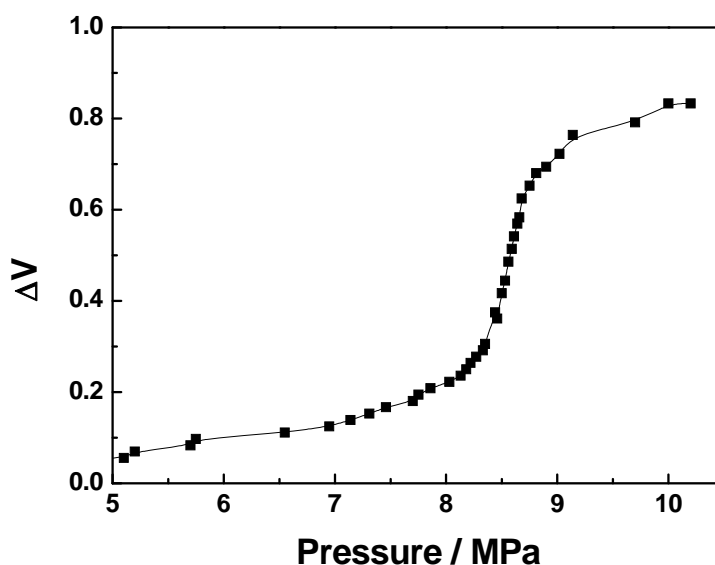


**Fig. 1.** A description of compatibility of EtOH with 'supercritical' CO<sub>2</sub> on CO<sub>2</sub> pressure. (T=40 °C, c=0.2 v/v)

### Effect of CO<sub>2</sub> Pressure on Coating Ratio and Yield

The dependence of the coating ratio for absorbing FeCl<sub>3</sub>/EtOH, and thereafter iron oxide yield on experimental pressure is shown in Fig. 2. The coating ratio increased in general with increasing pressure in the range from 14 to 22 MPa, then reached a plateau afterwards. In addition, a decreasing absorbing value from 10 to 14 MPa was concomitantly observed, which may partly result from the precursor's concentration inhomogeneity in the SCF' multiphase system at the lower pressure range, but the precise multiphase behavior and the mass transfer mechanism still need further investigation.

The elevated coating ratio and the consequent rise in yield with rising pressure are thus explained: CO<sub>2</sub> is a poorer solvent for the precursor at low pressure, and so only a limited amount of dissolved precursor can coat the cypress matrix, assisted by scCO<sub>2</sub>. With the increase of pressure, the limited amount increases, and the coating ratio rises, and this trend is maintained until the dissolution equilibrium of FeCl<sub>3</sub> in scCO<sub>2</sub>/EtOH has been obtained.

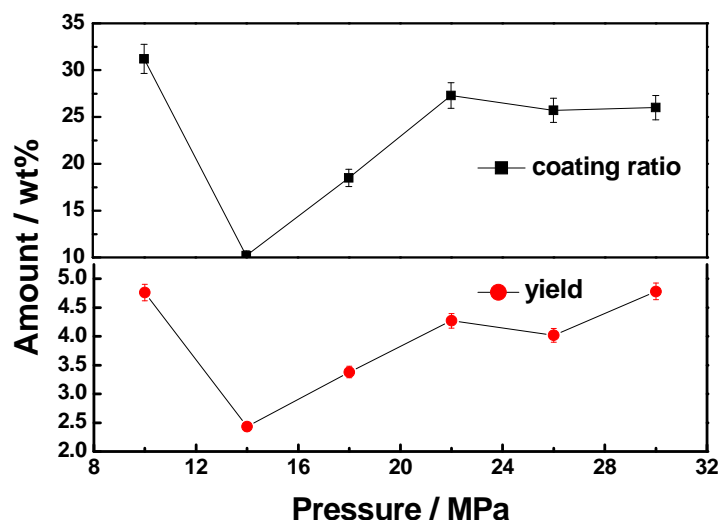
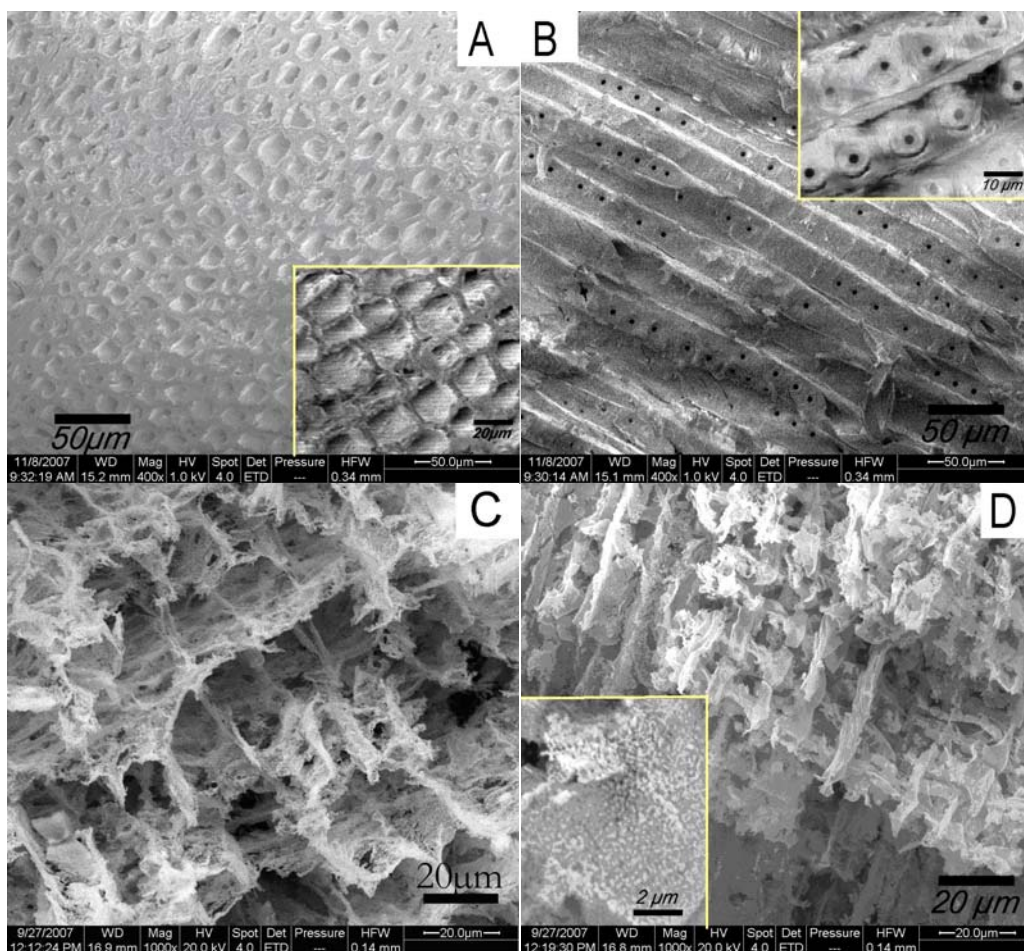


Fig. 2. The dependence of coating ratio and yield on scCO<sub>2</sub> pressure.

### Morphology of Porous Fe<sub>2</sub>O<sub>3</sub> and Fe<sub>2</sub>O<sub>3</sub>/SiO<sub>2</sub> composites

The brown iron oxide and its silica-based composite samples, obtained by calcination of the treated wood templates at 800 °C in air atmosphere for 3 h, retained the macroscopic shape of the corresponding cypress template with a bit of shrinkage in external dimensions. Moreover, the inherited microscopic structures of the cypress tissue were concomitantly retained in the iron oxide and its composite samples even after removal of the wood template. Figures 3a and 3b show the cross-sectional and longitudinal morphology of original cypress tissue scanned with no gold coating, 1.0 kV by SEM in high vacuum, and low-voltage modes. The well-aligned rectangle tracheids, and the transverse bordered pits of about 1 or 2 μm in the tracheid walls could be observed, which are channels connecting the different tracheid cells. Figures 3c and 3d show the transverse and oblique configurations of cypress-templated Fe<sub>2</sub>O<sub>3</sub> calcined at 800 °C taken by SEM. A well-aligned porous framework was observed at a μm scale. The pores originating from tracheids having diameters of about 15–20 μm were kept by the iron oxide. The above-mentioned images show an overall view, indicating that pores from tracheids are tubular and three-dimensional. The entire cellular structure was basically preserved, with adjacent tracheids linked together by middle lamellae. In addition to the macrocellular structure, the obtained iron oxide tissue also retained the detailed microstructure of the wood cells, the hollow vessels showed some tinier or finer microstructures, such as mesh-like cell wall replicas, and the rough and hollowed out inner-surface bricked up by iron oxide colloidal particles in the scale of about 100–200 nm (inserted part in Fig. 3d) were also obtained. In contrast, iron oxide replicas appeared much looser in form, which was noticeably different from our previous silica replica or the similar work by other scientists (Liu 2005); as may be attributed to our lesser impregnation amount of precursor into the matrix via the scCO<sub>2</sub> technique and specific hydrolyzation process.



**Fig. 3.** SEM images of the a) cross-section, b) axial section of cypress tissue, and c,d) oblique views of cypress-reproduced iron oxide porous samples calcined at 800 °C.

However, the inherited structure of iron oxide was relatively brittle, so the silica matrix was introduced for enhancing the strength as a framework, which may also have provided the benefit of depressing the transformation from  $\gamma$ - to  $\alpha$ - $\text{Fe}_2\text{O}_3$ , and achieving nanocomposites (Chanéac et al. 1995; Lund and Dumesic 1981; Savii et al. 2002; Ennas et al. 1999; Solinas et al. 2001). Figure 4 shows the SEM images of cypress-templated  $\text{SiO}_2$  (a&b),  $\text{Fe}_2\text{O}_3/\text{SiO}_2$  composite by Method #1 (c),  $\text{Fe}_2\text{O}_3$ -coated  $\text{SiO}_2$  composite by Method #2 (d&e) and #3 (f), which were all calcined at 800C. The conversion of wood tissue to inorganic materials, e.g.,  $\text{SiO}_2$ ,  $\text{Fe}_2\text{O}_3$ , and  $\text{SiO}_2/\text{Fe}_2\text{O}_3$  composites (Method #1 & #2) by biomineralization process, in general retained the morphology of cypress tissue. Rectangular tracheids replicas in the cypress-templated  $\text{SiO}_2$  sample were arranged compactly and orderly, as in the original softwood cypress tissue. Meanwhile the pores in the cell walls with a diameter ca. 1  $\mu\text{m}$  and 5 $\mu\text{m}$  remained respectively in the wood-templated  $\text{SiO}_2$  and its  $\text{Fe}_2\text{O}_3$  composite by method #1, which was different with that in Vogli et al.'s work (2001). These channels are able to connect the different cells and enhance their connectivity, as is advantageous for mass transfer in catalysis, absorption, etc. A phenomenon that couldn't be neglected was that the second-step replication for a  $\text{SiO}_2/\text{Fe}_2\text{O}_3$  composite using the silicified wood, i.e. the porous silica thereof, would

become crushed in an ammoniac hydrolyzing solution with ultrasonic vibration, so the macroscopical and microscopical structures were unfortunately both destroyed (Fig. 4f).

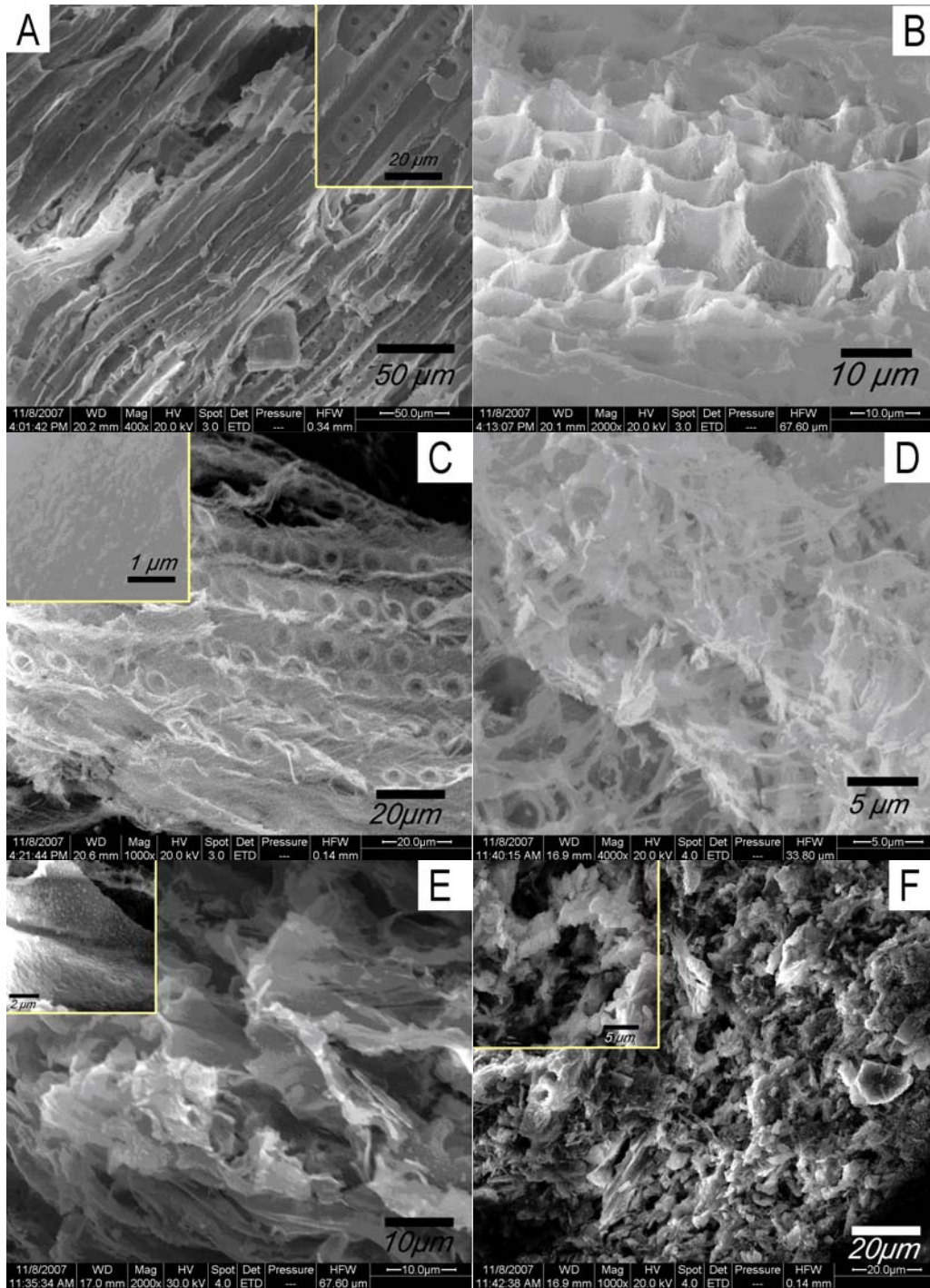


**Fig. 4.** SEM images of the a) longitudinal section, b) oblique view of cypress-templated  $\text{SiO}_2$ , c) longitudinal section of  $\text{Fe}_2\text{O}_3/\text{SiO}_2$  composite by Method #1, d, e)  $\text{Fe}_2\text{O}_3/\text{SiO}_2$  by Method #2, and f)  $\text{Fe}_2\text{O}_3/\text{SiO}_2$  by Method #3, which were all from calcination at  $800^\circ\text{C}$ .

### Porosity of Fe<sub>2</sub>O<sub>3</sub> and Fe<sub>2</sub>O<sub>3</sub>/SiO<sub>2</sub> Composites

Based on N<sub>2</sub> adsorption-desorption measurements, the isotherms and corresponding pore size distribution (PSD) curves for cypress-templated iron oxide and its silica-based composites calcined at 800 °C are shown in Fig. 5. As seen from the porous Fe<sub>2</sub>O<sub>3</sub> by different wood templates or pressure processes, the hysteresis loops were not so apparent (Fig. 5a). According to the IUPAC definitions, a IV-type curve is formed by mesopores (2–50 nm), and a II-type isotherm is attributed to macropores (>50 nm). At low relative pressure (<0.5), the nitrogen adsorbing action of macropores is the same as the monolayer adsorption of mesopores. But above medium relative pressure (>0.5), there is no capillary condensation phenomenon in macropores, and then no hysteresis loop. According to the types of isotherms and the PSD curves in Fig. 5b, the samples were identified that the BET surface area mainly was associated with mesopores in the range of 9–11 nm for porous Fe<sub>2</sub>O<sub>3</sub> products. Furthermore, the isotherms in Fig. 5, especially in Fig. 5a, were not typical according to IUPAC standards; this may be attributed the much lower surface area, especially from mesopores, in the hierarchically porous products in Fig. 5, i.e. the porous Fe<sub>2</sub>O<sub>3</sub>. (Some similar isotherms can also be seen in our peers' work, such as Liu et al. 2005; Fan et al. 2006.) However, with the introduction of a silica matrix, apparent loops were observed and the specific surface areas of the products were obviously augmented (Fig. 5c), (Li et al. 2001). We expect that such augmentation of surface area can enable potential applications in effective and selective catalysis.

The nm pores in the inorganic products may be attributed to the replication of nanofibers in the wood tissue, just as with the use of surfactants or liquid crystal molecules for a mesoporous material, and this process may be thus illustrated. When SCFs are used for precursor coating for an aerogel, removal of the template increases the pore volume (Wakayama and Fukushima 2000). From the nitrogen adsorption-desorption isotherms, the BET surface area of the porous iron oxides was calculated to be 8–19 m<sup>2</sup>/g, the total pore volume was found to be 22–45 mm<sup>3</sup>/g, and the PSD curves calculated by BJH method showed that the average pore diameter of the samples was 9–11 nm; and that for Fe<sub>2</sub>O<sub>3</sub>/SiO<sub>2</sub> composites were respectively 99–104 m<sup>2</sup>/g, 231–235 mm<sup>3</sup>/g, and 9 nm. In Table 1, the BET surface, total pore volume, and average mesopore size of porous iron oxide and its silica-based composites are summarized.

**Table 1.** Characterization of the Porosity of Porous Iron Oxide and its Silica-Based Composite Samples

Wood Template	Sur. Area (m <sup>2</sup> /g)	Pore Vol. (mm <sup>3</sup> /g)	Pore Diam. (nm)
Poplar (10 MPa)	12	27	9.0
Cypress (10 MPa)	19	45	9.4
Cypress (26 MPa)	8	22	10.9
Method #1	104	235	9.1
Method #2	99	231	9.3
Note: #1, Fe <sub>2</sub> O <sub>3</sub> /SiO <sub>2</sub> composite; #2, Fe <sub>2</sub> O <sub>3</sub> -coated SiO <sub>2</sub> blend.			

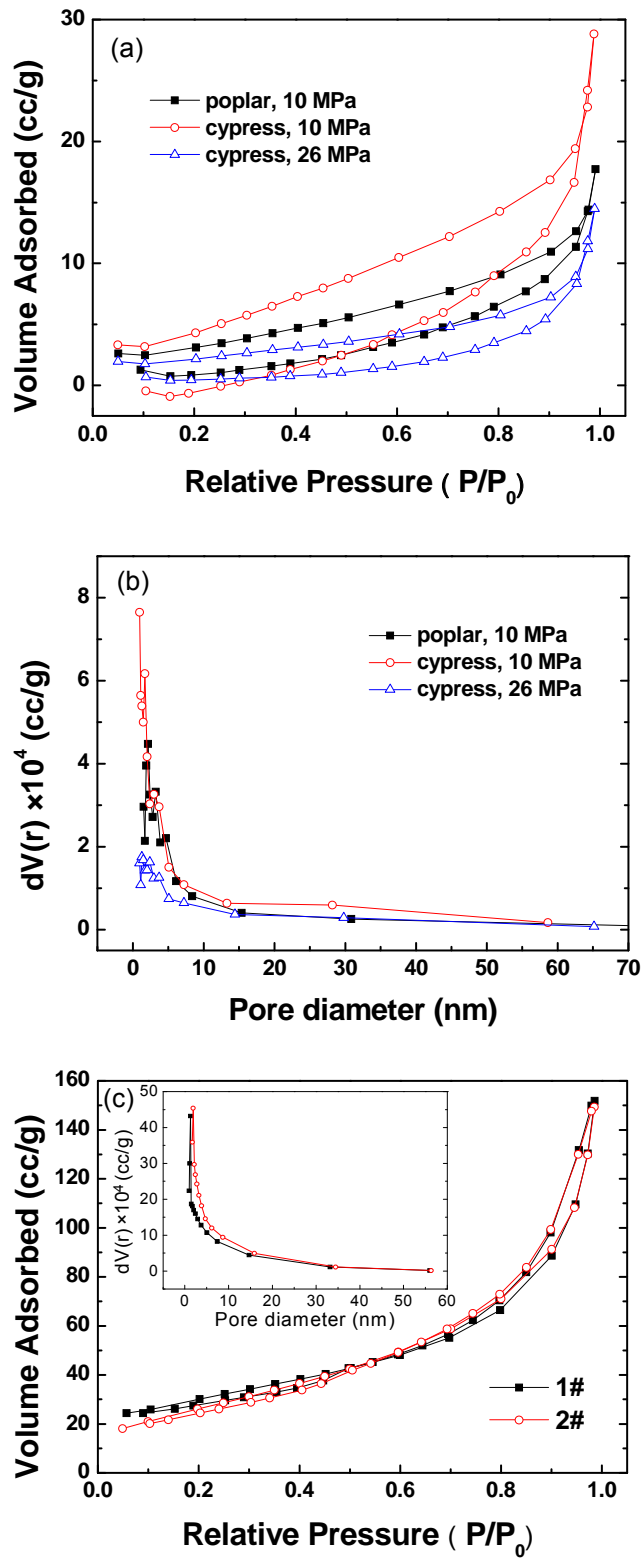


**Fig. 5.** N<sub>2</sub> adsorption-desorption isotherms and PSD curves for porous a,b) Fe<sub>2</sub>O<sub>3</sub> and c) SiO<sub>2</sub>/Fe<sub>2</sub>O<sub>3</sub> composite (by method #1 & #2) after removal of cypress template by calcination at 800 °C.

### XRD Analysis of $\text{Fe}_2\text{O}_3$ and $\text{Fe}_2\text{O}_3/\text{SiO}_2$ Composites

The samples were pulverized for powder X-ray diffraction. In Fig. 6, XRD patterns of all the iron oxide samples from different calcination temperatures are illustrated. According to these patterns, the original components of wood were removed, and the  $\alpha\text{-Fe}_2\text{O}_3$  was confirmed as the single phase. When the temperature rose, the peaks in the XRD pattern from the same wood template became sharper and more intense. Higher temperature led to an increase in the size of  $\alpha\text{-Fe}_2\text{O}_3$  crystallites, and good crystallinity was exhibited with the calcination temperature higher than  $800^\circ\text{C}$ .

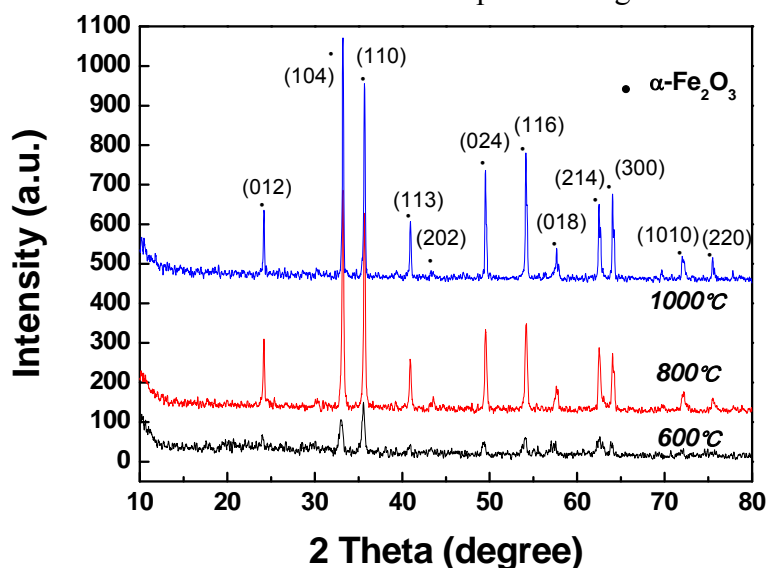


**Fig. 6.** XRD patterns of cypress-templated  $\text{Fe}_2\text{O}_3$  calcined at  $600^\circ\text{C}$ ,  $800^\circ\text{C}$ , and  $1000^\circ\text{C}$ . (Referenced JCPDS cards No. 330664 and 130534 )

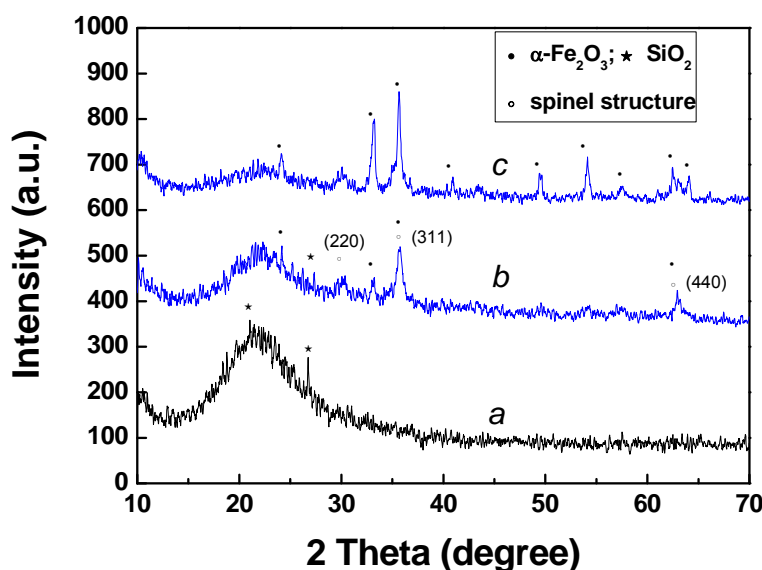


**Fig. 7.** XRD patterns of cypress-templated a)  $\text{SiO}_2$ , b)  $\text{Fe}_2\text{O}_3/\text{SiO}_2$  composite by Method #1, and c)  $\text{Fe}_2\text{O}_3$  coating  $\text{SiO}_2$  blend by Method #2 calcined at  $800^\circ\text{C}$ . (Referenced JCPDS cards No. 50490, 331161, 150026; 330664, 391346 )

X-ray diffraction spectra recorded for the different samples, referred to the compounding strategy that was used for iron oxide with silica matrix, are presented in Fig. 7. The XRD spectrum of A showed a new line at  $2\theta=26.74^\circ$ , which can be attributed to the  $\alpha$ -quartz phase (Ferreira da Silva and Valente 1998). The broad band between  $2\theta=20^\circ-27^\circ$ , which appeared in all XRD patterns, is due to the amorphous nature of the silica matrix (del Monte 1997; Zhang 1997). A significant decrease of diffraction line intensity of  $\alpha$ -Fe<sub>2</sub>O<sub>3</sub> is observed in Sample B, i.e. the Fe<sub>2</sub>O<sub>3</sub>/SiO<sub>2</sub> composite; the compounding of the silica and iron oxide limited the growth of  $\alpha$ -Fe<sub>2</sub>O<sub>3</sub> particle size in the binary composite system. An analogous process is illustrated in the case of the hematite phase transforming into an iron-rich spinel phase and some of the iron atoms reacting with the amorphous SiO<sub>2</sub>, forming a new Fe(II)-containing silicate compound (Jiang 1996). From the characteristic diffraction line of Sample C, Fe<sub>2</sub>O<sub>3</sub> coating SiO<sub>2</sub>,  $\alpha$ -Fe<sub>2</sub>O<sub>3</sub> seemed almost to be the only phase evidenced by XRD. This could be an indication that the silica was well coated by the iron oxide layer with all iron atoms found in a hematite phase. In addition, the pattern of the sample C showed well-crystalline  $\alpha$ -Fe<sub>2</sub>O<sub>3</sub>, with a trace of amorphous SiO<sub>2</sub>, which enhances the background around  $20^\circ-30^\circ$  (Jiang 1996).

Because of the much higher calcination temperatures than  $\sim 350^\circ\text{C}$  (Ennas et al. 1998, 1999; Chanéac et al. 1995) and the system of the composites that are richer in oxygen, a  $\gamma$ -Fe<sub>2</sub>O<sub>3</sub> phase, or a transformation process of  $\gamma$ - to  $\alpha$ -Fe<sub>2</sub>O<sub>3</sub>, was not apparent (Savii et al. 2002; Cannas et al. 1998, 1999, 2001; Solinas et al. 2001), but there was still a trace of spinel structure, i.e. maghemite  $\gamma$ -Fe<sub>2</sub>O<sub>3</sub> phase, which was observed in the Fe<sub>2</sub>O<sub>3</sub>/SiO<sub>2</sub> composite, as seen in Fig. 7b & c (Jing & Wu 2004; Ortega et al. 2006). By introduction of silica into iron oxide, the diffraction peaks of  $\alpha$ -Fe<sub>2</sub>O<sub>3</sub> lost intensity and broadened significantly in hematite-amorphous silica composite (by Method #1). Usually no interaction between the metal oxide nanoparticles and the silica network forms during the sol-gel process (Corrias 2000), but the mixing of silica into iron oxide changed the phase behaviors and the properties thereof. In general, the introduction of silica may make full use of the advantages of the catalysis property of iron oxide, and the strengthened magnetization by maghemite phase may help the better separation of the heterogeneous catalyst.

## CONCLUSION

The syntheses of hierarchically porous  $\alpha$ -Fe<sub>2</sub>O<sub>3</sub> and the corresponding SiO<sub>2</sub>-based mixed composites with a relatively green and highly efficient process were demonstrated, replicating the macroscopic shape as well as nanoscale and microscale structures of cypress tissue template. The introduction of silica into iron oxide enhanced the strength of the product as well as the surface area; even the crystalline phase transformation was restricted. For example, the BET surface area of the porous iron oxides was calculated to be 8–19 m<sup>2</sup>/g, and that for Fe<sub>2</sub>O<sub>3</sub>/SiO<sub>2</sub> composites was in the range of 99–104 m<sup>2</sup>/g; the pure iron oxides showed a crystalline structure of  $\alpha$ -Fe<sub>2</sub>O<sub>3</sub>, but the introduction of amorphous silica restricted the growth model of the crystalline structure, and a trace of  $\gamma$ -

Fe<sub>2</sub>O<sub>3</sub> phase was revealed. Furthermore, a supercritical fluid was shown to be an effective solvent for the microstructures replication to produce hierarchical materials with designed macroscopic shapes, which would provide a novel and important perspective on biomineralization and the like. The process can be applied over a range of structural or functional ceramics or metals, of which structures and properties may be skillfully controlled through the choice of templates, precursors, and other aided techniques, which may have potential application in further building functional materials such as catalysts, sorbents, magnets, and sensors.

## ACKNOWLEDGMENTS

We are grateful for the financial support from the Prominent Research Talents in University of Henan Province, the National Natural Science Foundation of China (No. 20404012) and the Prominent Youth Science Foundation of Henan Province (No. 0512001200).

## REFERENCES CITED

- Cabañas, A., Enciso, E., Carbajo, M., Torralvo, M., Pando, C., and Renuncio, J. (2005). "Synthesis of ordered macroporous SiO<sub>2</sub> in supercritical CO<sub>2</sub> using 3D-latex array templates," *Chem. Commun.* 2618-2620.
- Cannas, C., Concas, G., Falqui, A., Musinu, A., Spano, G., and Piccaluga, G. (2001). "Investigation of the precursors of  $\gamma$ -Fe<sub>2</sub>O<sub>3</sub> in Fe<sub>2</sub>O<sub>3</sub>/SiO<sub>2</sub> nanocomposites obtained through sol-gel," *J. Non-Cryst. Solids* 286(1-2), 64-73.
- Cannas, C., Concas, G., Musinu, A., Piccaluga, G., and Spano, G. (1999). "Mössbauer spectroscopic study of Fe<sub>2</sub>O<sub>3</sub> nanoparticles dispersed over a silica matrix," *Z. Naturforsch.* 54a, 513-518.
- Cannas, C., Gatteschi, D., Musinu, A., Piccaluga, G., and Sangregorio, C. (1998). "Structural and magnetic properties of Fe<sub>2</sub>O<sub>3</sub> nanoparticles dispersed over a silica matrix," *J. Phys. Chem. B* 102(40), 7721-7726.
- Chanéac, C., Tronc, E., and Jolivet, J. (1995). "Nanoparticles prepared by sol-gel method," *Nanostruct. Mater.* 6, 715-719.
- Chen, H., and Sachtler, W. (1998). "Activity and durability of Fe/ZSM-5 catalysts for lean burn NO<sub>x</sub> reduction in the presence of water vapor," *Catal. Today* 42(1-2), 73-83.
- Cooper, A. (2003). "Porous materials and supercritical fluids," *Adv. Mater.* 15(13), 1049-1059.
- Cornell, R., and Schwertmann, U. (1996). *The Iron Oxides: Structure, Properties, Reactions, Occurrence and Uses*, VCH Verlagsgesellschaft, Weinheim, Germany.
- Corrias, A., Ennas, G., Mountjoy, G., and Paschina, G. (2000). "An X-ray absorption spectroscopy study of the Fe K edge in nanosized maghemite and in Fe<sub>2</sub>O<sub>3</sub>-SiO<sub>2</sub> nanocomposites," *Phys. Chem. Chem. Phys.* 2, 1045-1050.
- Darr, J., and Poliakov, M. (1999). "New directions in inorganic and metal-organic coordination chemistry in supercritical fluids," *Chem. Rev.* 99(2), 495-542.

- del Monte, F., Morales, M., Levy, D., Fernandez, A., Ocaña, M., Roig, A., Molins, E., O'Grady, K., and Serna, C. (1997). "Formation of  $\gamma$ -Fe<sub>2</sub>O<sub>3</sub> isolated nanoparticles in a silica matrix," *Langmuir* 13(14), 3627-3634.
- Dong, A., Wang, Y., Tang, Y., Ren, N., Zhang, Y., Yue, Y., and Gao, Z. (2002). "Zeolitic tissue through wood cell templating," *Adv. Mater.* 14(12), 926-929.
- Ennas, G., Marongiu, G., Musinu, A., Falqui, A., Ballirano, P., and Caminiti R. (1999). "Characterization of nanocrystalline  $\gamma$ -Fe<sub>2</sub>O<sub>3</sub> prepared by wet chemical method," *J. Mater. Res.* 14(4), 1570-1575.
- Ennas, G., Musinu, A., Piccaluga, G., Zedda, D., Gatteschi, D., Sangregorio, C., Stanger, J., Concas, G., and Spano, G. (1998). "Characterization of iron oxide nanoparticles in an Fe<sub>2</sub>O<sub>3</sub>-SiO<sub>2</sub> composite prepared by a sol-gel method," *Chem. Mater.* 10(2), 495-502.
- Fan, T., Li, X., Liu, Z., Gu, J., Zhang, D., and Guo, Q. (2006). "Microstructure and infrared absorption of biomorphic chromium oxides templated by wood tissues," *J. Am. Ceram. Soc.* 89(11), 3511-3515.
- Ferreira da Silva, M., and Valente, M. (1998). "Crystallization and properties of sol-gel derived 10Fe<sub>2</sub>O<sub>3</sub>-10Al<sub>2</sub>O<sub>3</sub>-80SiO<sub>2</sub> glass-ceramics," *J. Non-Cryst. Solids* 232-234(11), 409-415.
- Fukushima, Y., and Wakayama, H. (1999). "Nanoscale casting using supercritical fluid," *J. Phys. Chem. B* 103(16), 3062-3064.
- Jiang, J., Zhou, Y., Mørup, S., and Bender Koch, C. (1996). "Microstructural evolution during high energy ball milling of Fe<sub>2</sub>O<sub>3</sub>-SiO<sub>2</sub> powders," *Nanostruct. Mater.* 7(4), 401-410.
- Jing, Z., and Wu, S. (2004). "Synthesis, characterization and magnetic properties of  $\gamma$ -Fe<sub>2</sub>O<sub>3</sub> nanoparticles via a non-aqueous medium," *J. Solid State Chem.* 177, 1213-1218.
- Johnston, K., and Shah, P. (2004). "Making nanoscale materials with supercritical fluids," *Science* 303, 482-483.
- Jolivet, J. (2000). "Metal Oxide Chemistry and Synthesis," J. Wiley and Sons Ltd., Chichester, UK.
- Li, D., Wu, D., Wang, X., Lu, L., and Yang, X. (2001). "Rapid preparation of porous Fe<sub>2</sub>O<sub>3</sub>/SiO<sub>2</sub> nanocomposites via an organic precursor," *Mater. Res. Bull.* 36, 2437-2442.
- Liu, Z., Fan, T., Zhang, W., and Zhang, D. (2005). "The synthesis of hierarchical porous iron oxide with wood templates," *Micropor. Mesopor. Mater.* 85(1-2), 82-88.
- Lund, C., and Dumesic, J. (1981). "Strong oxide-oxide interactions in silica-supported magnetite catalysts. 1. X-ray diffraction and Mössbauer spectroscopy evidence for interaction," *J. Phys. Chem.* 85(21), 3175-3180.
- Ni, W., Chen, J., and Xu, Q. (2008). "Synthesis and characterization of hierarchically porous silica with poplar tissue as template with assistance of supercritical CO<sub>2</sub>," *BioRes.* 3(2), 461-476.
- Ortega, D., Garitaonandia, J., Barrera-Solano, C., Ramírez-del-Solar, M., Blanco, E., and Domínguez, M. (2006). " $\gamma$ -Fe<sub>2</sub>O<sub>3</sub>/SiO<sub>2</sub> nanocomposites for magneto-optical applications: Nanostructural and magnetic properties," *J. Non-Cryst. Solids* 352(26-27), 2801-2810.

- Panov, G., Uriarte, A., Rodkin, M., and Sobolev, V. (1998). "Generation of active oxygen species on solid surfaces. Opportunity for novel oxidation technologies over zeolites," *Catal. Today* 41(4), 365-385.
- Poliakoff, M., Fitzpatrick, J., Farren, T., and Anastas, P. (2002). "Green chemistry: Science and politics of change," *Science* 297(5582), 807-810.
- Savii, C., Popovici, M., Enache, C., Subrt, J., Niznansky, D., Bakardzieva, S., Caizer, C., and Hrianca, I. (2002). "Fe<sub>2</sub>O<sub>3</sub>-SiO<sub>2</sub> composites obtained by sol-gel synthesis," *Solid State Ionics* 151(1-4), 219-227.
- Solinas, S., Piccaluga, G., Morales, M., and Serna, C. (2001). "Sol-gel formation of  $\gamma$ -Fe<sub>2</sub>O<sub>3</sub>/SiO<sub>2</sub> nanocomposites," *Acta Mater.* 49(14), 2805-2811.
- Tirrell, D., Baer, E., Calvert, P., Cappello, J., Dimarzio, E., Evans, E., et al. (1994). "Hierarchical structure in biology as a guide for new materials technology," National Academy Press, Washington DC.
- Vogli, E., Mukerji, J., Hoffman, C., Kladny, R., Sieber, H., and Greil P. (2001). "Conversion of oak to cellular silicon carbide ceramic by gas-phase reaction with silicon monoxide," *J. Am. Ceram. Soc.* 84(6), 1236-1240.
- Wakayama, H., and Fukushima, Y. (1999). "Porous platinum fibers synthesized using supercritical fluid," *Chem. Commun.* 391-392.
- Wakayama, H., and Fukushima, Y. (2000). "Nanoporous silica prepared with activated carbon molds using supercritical CO<sub>2</sub>," *Chem. Mater.* 12(3), 756-761.
- Wang, S., Wang, W., Wang, W., Jiao, Z., Liu, J., and Qian, Y. (2000). "Characterization and gas-sensing properties of nanocrystalline iron(III) oxide films prepared by ultrasonic spray pyrolysis on silicon," *Sens. Actuators B* 69(1-2), 22-27.
- Ying, J., Mehnert, C., and Wong, M. (1999). "Synthesis and applications of supramolecular-templated mesoporous materials," *Angew. Chem. Int. Ed.* 38(1-2), 56-77.
- Zhang, L., Papaefthymiou, G., and Ying, J. (1997). "Size quantization and interfacial effects on a novel  $\gamma$ -Fe<sub>2</sub>O<sub>3</sub>/SiO<sub>2</sub> magnetic nanocomposite via sol-gel matrix-mediated synthesis," *J. Appl. Phys.* 81(10), 6892-6900.

Article submitted: April 16, 2008; Peer-review completed: June 3, 2008; Revised version received and accepted: June 16, 2008; Published June 18, 2008.